Acta Cryst C STRUCTURAL CHEMISTRY
ISSN 2053-2296

Thermal-induced transformation of glutamic acid to pyroglutamic acid and self-cocrystallization: a charge–density analysis

Sehrish Akram,[a] Arshad Mehmood,[b] Sajida Noureen[a]* and Maqsood Ahmed[a]*

[a]Materials Chemistry Laboratory, Institute of Chemistry, The Islamia University of Bahawalpur, Baghdad-ul-Jadeed Campus 63100, Pakistan, and [b]Department of Chemistry and Biochemistry, Texas Christian University, Fort Worth, Texas 76129, USA. *Correspondence e-mail: sajida.noureen@iub.edu.pk, maqsood.ahmed@iub.edu.pk

Received 7 September 2021
Accepted 27 December 2021

Edited by A. Lemmerer, University of the Witwatersrand, South Africa

Keywords: glutamic acid; pyroglutamic acid; *MoPro*; cocrystal; ELMAM2; crystal structure; transferability principle.

CCDC references: 2097833; 2097831

Supporting information: this article has supporting information at journals.iucr.org/c

Thermal-induced transformation of glutamic acid to pyroglutamic acid is well known. However, confusion remains over the exact temperature at which this happens. Moreover, no diffraction data are available to support the transition. In this article, we make a systematic investigation involving thermal analysis, hot-stage microscopy and single-crystal X-ray diffraction to study a one-pot thermal transition of glutamic acid to pyroglutamic acid and subsequent self-cocrystallization between the product (hydrated pyroglutamic acid) and the unreacted precursor (glutamic acid). The melt upon cooling gave a robust cocrystal, namely, glutamic acid–pyroglutamic acid–water (1/1/1), $C_5H_7NO_3$·-$C_5H_9NO_4$·H_2O, whose structure has been elucidated from single-crystal X-ray diffraction data collected at room temperature. A three-dimensional network of strong hydrogen bonds has been found. A Hirshfeld surface analysis was carried out to make a quantitative estimation of the intermolecular interactions. In order to gain insight into the strength and stability of the cocrystal, the *transferability principle* was utilized to make a topological analysis and to study the electron-density-derived properties. The *transferred* model has been found to be superior to the classical independent atom model (IAM). The experimental results have been compared with results from a multipolar refinement carried out using theoretical structure factors generated from density functional theory (DFT) calculations. Very strong classical hydrogen bonds drive the cocrystallization and lend stability to the resulting cocrystal. Important conclusions have been drawn about this transition.

1. Introduction

Glutamic acid has been known to undergo dehydration to transform into pyroglutamic acid through internal cyclization upon heating to 175–190 °C (Haitinger, 1882; Menozzi & Appiani, 1892, 1894; He *et al.*, 2003). This conversion has been studied with respect to a range of conditions, such as temperature and pH (Wilson & Cannan, 1937). The resultant lactam has biological importance and finds use in the pharmaceutical industry, in the area of skin therapeutics (Gibson & Scott, 1992). Pharmacologically, pyroglutamic acid is more stable and can be converted into glutamic acid only under harsh conditions (Shih, 1985). Therefore, many peptide-based pharmaceuticals contain pyroglutamic acid instead of glutamic acid, for example, bombesin, sauvagin and gastrin (Suzuki *et al.*, 1999). Mosqueira *et al.* (2008) suggested the inner cyclization mechanism of glutamic acid into pyroglutamic acid by the removal of a water molecule. In a recent study, the cyclization product was characterized using different techniques [quadrupole mass spectrometry (QMS), differential scanning calorimetry (DSC) and thermogravimetric analysis (TGA)] and the results showed that dehydration occurs at 200 °C

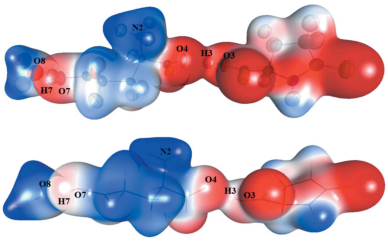

(Weiss *et al.*, 2018). To the best of our knowledge, no three-dimensional structural data are available to support this cyclization. Although a cocrystal of glutamic acid and pyroglutamic acid has been reported (Taira & Watson, 1977), it was grown from a 1:1 mixture of the individual compounds in aqueous solution. In this article, we report a one-pot thermal-induced cyclization and self-cocrystallization of glutamic acid and pyroglutamic acid. Glutamic acid, which is known to exist as a zwitterion (2-azaniumyl-4-carboxybutanoate) at pH values in the range 2.5–4.1 (Neuberger, 1936), is believed to play a significant role in this cocrystallization (Nugrahani & Jessica, 2021). A topological analysis of the intermolecular interactions and electrostatic forces in pure glutamic acid and its various solid forms has been made previously (Flaig *et al.*, 1999, 2002; Ciunik & Głowiak, 1983; Nagashima *et al.*, 1992*a*,*b*; Sano *et al.*, 1989).

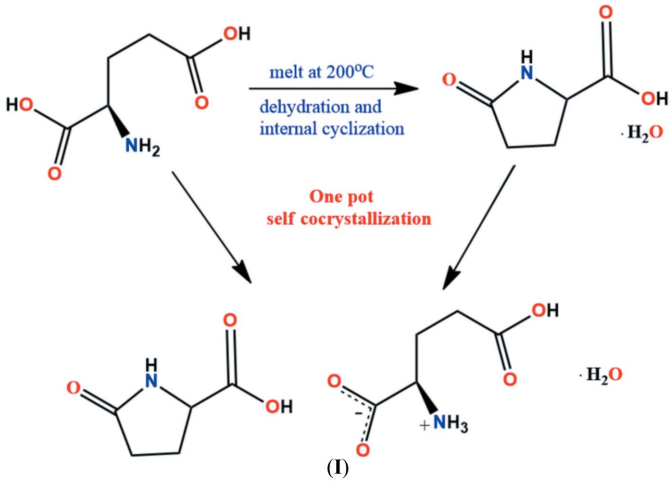

Scheme 1

We have determined the three-dimensional structure of the resulting cocrystal hydrate by single-crystal diffraction analysis. A thorough understanding of the intermolecular interactions and electrostatic forces is necessary to comprehend how the cocrystallization is driven. The classically used Independent Atomic Model (IAM) does not provide detailed information about these interactions due to systematic errors in the refinement model (Ruysink & Vos, 1974). Instead, a multipolar model is needed for a detailed modelling of the electron-density distribution in the crystal. However, the latter requires high-resolution ($d \leq 0.5$ Å) data (Coppens, 1998) collected at low temperature, which usually cannot be expected from every crystal and not every laboratory possesses a low-temperature facility. However, the *transferability principle* provides a low cost but reliable solution to this problem. This principle was first tested by Brock *et al.* (1991) by transferring the atomic electron-density parameters from high-resolution data of perylene to low-resolution diffracted data of naphthalene and anthracene. This work was further extended by Pichon-Pesme *et al.* (1995) to design the first experimental database of protein fragments, known as the experimental library of multipolar atomic model (ELMAM), based on the Hansen & Coppens (1978) multipolar atomic parameter. In addition, two other theoretical databases of pseudoatoms are also available, namely, the Invariom database (Dittrich *et al.*, 2004) and the University at Buffalo Pseudoatom Database (UBDB) (Volkov *et al.*, 2004) based on the same multipolar formalism. These databases have been updated several times, for example, ELMAM was updated (Pichon-Pesme *et al.*, 2004) and then modified to the ELMAM2 library (Domagała *et al.*, 2012); the ELMAM database is restricted mostly to protein atoms, while the ELMAM2 library is extended to common functional groups encountered in organic molecules and is based on optimized local axes systems (Domagała *et al.*, 2008, 2012). The use of these databases has been highlighted in many examples of crystallographic modelling (Pichon-Pesme *et al.*, 1995; Dittrich *et al.*, 2004, 2005, 2007; Jelsch *et al.*, 1998; Ahmed *et al.*, 2011; Faroque *et al.*, 2019; Shahi *et al.*, 2020).

In the current study, we present three-dimensional structural evidence of the thermal-induced transformation of glutamic acid to pyroglutamic acid monohydrate and serendipitously discovered self-cocrystallization between the two components by single-crystal X-ray diffraction. In order to gain insight into the mechanism and stability of the resulting cocrystal, (**I**), we have made a topological analysis of the intermolecular interactions and studied the electrostatic forces by transferring electron-density parameters from the ELMAM2 library (Domagała *et al.*, 2012). Furthermore, the experimental results have been compared with a model refined using theoretical structure factors.

2. Experimental

2.1. Material

L-Glutamic acid (2-aminopentanedioic acid) was obtained from Sigma–Aldrich and used without further purification.

2.2. Thermal analysis

Thermal analysis was conducted with a PerkinElmer STA 6000 simultaneous TGA/DSC instrument. Approximately 11 mg of pure L-glutamic acid was placed in a ceramic crucible. The sample was heated at a rate of 5 °C min^{-1} from 25 to 400 °C. Nitrogen was used as the purge gas at a rate of 20 ml min^{-1} (Fig. 1).

2.3. Hot-stage microscopy

Hot-stage microscopy was performed on an Instec HSC302 heating stage attached to an Olympus SZX10 polarizing microscope fitted with a DP74 camera. In the light of the thermal analysis, the heating experiment was conducted to 215 °C only (see video in the supporting information).

2.4. Single-crystal growth by melt cocrystallization

Crystals were grown *via* a melt crystallization procedure in the light of the thermal profile. For this purpose, a few micrograms of pure glutamic acid were heated slowly to 200 °C and the temperature was maintained at 200 °C for a few minutes. Afterwards, the melt was allowed to cool to room

Table 1
Experimental details.

Crystal data	
Chemical formula	$C_5H_7NO_3{\cdot}C_5H_9NO_4{\cdot}H_2O$
M_r	294.26
Crystal system, space group	Monoclinic, $P2_1$
Temperature (K)	298
a, b, c (Å)	5.1153 (3), 7.1849 (4), 18.4639 (9)
β (°)	96.817 (2)
V (Å^3)	673.80 (6)
Z	2
Radiation type	Mo $K\alpha$
μ (mm^{-1})	0.13
Crystal size (mm)	0.5 × 0.29 × 0.07
Data collection	
Diffractometer	Bruker D8 Venture
Absorption correction	Multi-scan (*SADABS*; Bruker, 2016; Krause *et al.*, 2015)
T_{min}, T_{max}	0.487, 0.745
No. of measured, independent and observed [$I \geq 2\sigma(I)$] reflections	7139, 2442, 1905
R_{int}	0.055
(sin $\theta/\lambda)_{max}$ (Å^{-1})	0.602
Refinement (IAM *SHELX*)	
$R[F^2 > 2\sigma(F^2)]$, $wR(F^2)$, S	0.051, 0.116, 1.12
No. of reflections	2442
No. of parameters	199
No. of restraints	1
H-atom treatment	H atoms treated by a mixture of independent and constrained refinement
$\Delta\rho_{max}$, $\Delta\rho_{min}$ (e Å^{-3})	0.27, −0.27
Absolute structure	Flack (1983)
Absolute structure parameter	0.0 (19)
Refinement (ELMAM2)	
$R[F^2 > 2\sigma(F^2)]$, $wR(F^2)$, S	0.045, 0.086, 0.88
No. of parameters	120
H-atom treatment	H-atom parameters constrained to DFT-optimized values
$\Delta\rho_{max}$, $\Delta\rho_{min}$ (e Å^{-3})	0.24, −0.25
Refinement (Theoretical)	
$R[F^2 > 2\sigma(F^2)]$, $wR(F^2)$, S	0.003, 0.003, 1.05
No. of parameters	336
H-atom treatment	H-atom parameters constrained to DFT-optimized values
$\Delta\rho_{max}$, $\Delta\rho_{min}$ (e Å^{-3})	0.24, −0.24

Computer programs: *SAINT* (Bruker, 2016), *SHELXT2018* (Sheldrick, 2015), *olex2.refine* (Bourhis *et al.*, 2015) and *OLEX2* (Dolomanov *et al.*, 2009).

temperature. Plate-like crystals were obtained (see Fig. S1 in the supporting information).

2.5. Single-crystal X-ray diffraction (SCXRD)

Crystal data, data collection and structure refinement details of the GluA–PyroGluA–H_2O (1/1/1) cocrystal are summarized in Table 1. The crystals were generally found to be diffusely diffracting. A good-quality single crystal (see Fig. S1 in the supporting information) was chosen under an Olympus SZX10 polarizing microscope and was mounted on the goniometer head. The diffraction data were collected on a Bruker D8 Venture with a PHOTON II detector single-crystal X-ray diffractometer at room temperature (25 °C) using Mo $K\alpha$ radiation (λ = 0.71073 Å).

2.5.1. IAM *SHELX* refinement. The GluA–PyroGluA–H_2O (1/1/1) cocrystal was solved in the space group $P2_1$ using *OLEX2* software (Dolomanov *et al.*, 2009) by direct methods. For the initial independent atomic model (IAM) refinement, *SHELXL* (Sheldrick, 2008) in the *OLEX2* software package was used. All the H atoms were located in a difference Fourier map and the riding model was used for the H atoms bonded to C atoms. At the end of the *SHELXL* IAM refinement, the R factor was 0.051, the wR factor was 0.116 and the goodness-of-fit S was 1.12. The maximum and minimum electron-density peaks were at 0.27 and 0.27 e Å^{-3}, respectively.

2.5.2. *MoPro* refinement. The structural information obtained from the *SHELX* refinement was imported into the *MoPro* (*MoPro_1805_win*) software package (Jelsch *et al.*, 2005). The scale factor was refined initially and then the positions (x, y and z), as well as their displacement parameters (U_{ij}), were refined using all data. The C—H bond lengths were then constrained to DFT-optimized (DFT is density functional theory) distances (the procedure will be described in the following sections).

The electron-density parameters of the Hansen & Coppens (1978) model from the ELMAM2 library were transferred using *MoPro* software (Jelsch *et al.*, 2005) and keeping the asymmetric unit electrically neutralized. Only the scale factor, position and displacement parameters were refined until convergence, while all the multipolar parameters were kept fixed and constant. After the ELMAM2 refinement, the R, wR and S parameters changed to 0.045, 0.086 and 0.88, respectively. The highest and lowest electron-density peaks were at 0.24 and −0.25 e Å^{-3}.

2.6. Theoretical calculations

Two types of DFT calculations were performed.

In the *first step*, the coordinates of H atoms only were optimized using periodic DFT-D3 calculations starting with the atomic positions and lattice parameters obtained from *MoPro* IAM refinements converged with the standard neutron distances. The process of optimization was terminated when the forces on the atoms and the threshold on the total energy were less than 10^{-4} and 10^{-7} a.u., respectively. Calculations used the *Quantum Espresso* (QE; Giannozzi *et al.*, 2017) suite of programs. Ultrasoft pseudopotentials were employed for all atoms using the Perdew–Burke–Ernzerh (PBE) (Perdew *et al.*, 1996) exchange–correlation functional in combination with Grimme's D3 correction for dispersion interactions (Grimme *et al.*, 2010). The cut-off energy and the electronic density of plane waves were set at 70 and 840 Ry, respectively. The mesh of the unit cell for k-point sampling was set at 12 × 8 × 2, which corresponds to ∼0.1 Å of k-space resolution. To achieve self-consistency, a mixing factor of 0.7 was used during the calculations. The obtained optimized H-atom distances were used for further *MoPro* ELMAM2 and multipolar refinements using theoretical structure factors.

In the *second step*, a single-point energy calculation was performed on the final coordinates obtained after the multipolar refinement using the all-electron frozen-core PAW

Table 2
Hydrogen-bond geometry (Å, °) of (**I**) for the ELMAM2 model arranged on the basis of increasing hydrogen-bond distance.

D—H···*A*	*D*—H	H···*A*	*D*···*A*	*D*—H···*A*
O3—H3···O4	1.03	1.53	2.5535	173
O7—H7···O8	1.03	1.57	2.5825	169
N2—H2*c*···O5^{iii}	1.04	1.78	2.8087	169
O8—H8*c*···O1^{vi}	0.99	1.79	2.7346	158
N2—H2*b*···O5^{vii}	1.05	1.79	2.8369	170
N2—H2*a*···O2^{v}	1.04	1.82	2.8566	174
O8—H8*d*···O1^{v}	0.99	1.82	2.7485	156
N1—H1···O7^{iv}	1.02	2.27	3.2218	156
O3—H3···C6	1.03	2.39	3.3599	157
C7—H7*a*···O6	1.09	2.50	3.1153	115
C2—H2*e*···O1^{ii}	1.10	2.51	3.4914	148
C8—H8*a*···O3^{i}	1.09	2.56	3.4705	141
O8—H8*c*···O1^{vi}	0.99	2.70	3.5045	139

Symmetry codes: (i) $-x-1, y-\frac{1}{2}, -z-1$; (ii) $-x-1, y+\frac{1}{2}, -z-2$; (iii) $-x-1, y+\frac{1}{2}, -z-1$; (iv) $-x, y-\frac{1}{2}, -z-1$; (v) $-x, y+\frac{1}{2}, -z-1$; (vi) $x, y, z+1$; (vii) $x+1, y, z$.

(Blöchl, 1994) methodology on a dense real-space grid comprising 180 × 360 × 432 points along the crystallographic axes. The PBE exchange–correlation approximation was used with the same *k*-point sampling adopted for the partial geometry optimization. The theoretical structure factors in the experimental sin (θ)/λ limits were obtained by the Fourier transform of the calculated total electron-density grid using a Python script developed by one of the authors (AM). The multipolar refinement of scale factors and electron-density parameters was performed using the obtained static structure factors by excluding the refinement of atomic positions and setting the displacement parameters of the atoms to zero.

The integration of electron density was performed using the *WinXPRO* suite (Stash & Tsirelson, 2014) to obtain the atomic charges and volumes from both the experimental and the theoretical refinement models.

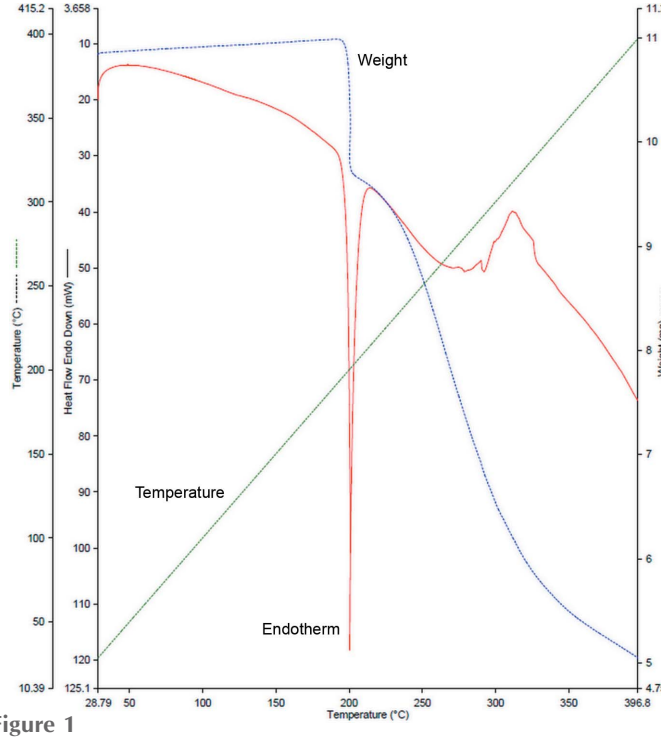

Figure 1
TGA/DSC analysis showing the weight loss and melting point of L-glutamic acid.

3. Results and discussion

3.1. Thermal analysis and hot-stage microscopy of L-glutamic acid

The thermal decomposition profile of L-glutamic acid is in agreement with that reported by Weiss *et al.* (2018). The sample remains stable up to 200 °C, followed by a sharp endothermic peak at 200 °C (Fig. 1), which indicates the melting of the acid. This is followed by a weight loss of around 12%, indicating dehydration. In order to monitor the changes, we performed hot-stage microscopy, as can be seen in a video (see supporting information), which shows the events between 195 and 215 °C. The crystal remains intact until the melting point but then the phase shift within the crystal becomes visible and exerts some degree of mechanical force as the crystal shows displacement. During the melting process, bubbles emerge, which are presumably water as by-product. Hence, it can be concluded that internal conversion is synchronous with the melting process.

3.2. Crystal structure analysis

3.2.1. GluA–PyroGluA–H_2O (1/1/1) cocrystal. The asymmetric unit of the cocrystal ($P2_1$) consists of one pyroglutamic acid molecule, one glutamic acid molecule and one water molecule forming the catemeric motif shown in Fig. 2 from the ELMAM2 model.

This catemeric cocrystal is stabilized *via* a three-dimensional network of classical O—H···O and N—H···O hydrogen bonds as a result of the zwitterionic effect of glutamic acid, in which the O4 atom is deprotonated by transfer of its proton to atom N2. A survey of the Cambridge Structural Database (CSD, Version 2.0 of 2020; Groom *et al.*, 2016) reveals that the O5—C6—C7—N2 torsion angle exists over a very wide range (148–179°) due to the possibility of free rotation around the C6—C7 single bond. Similarly, the O3—C5—C4—N1 torsion angle, calculated between the carboxyl group and the pyrrole ring of pyroglutamic acid, is 174.5 (2)°, which indicates that the carboxyl group is not coplanar with the pyrrole ring. The crystal shows a zigzag arrangement along the *b* axis (Fig. 3).

3.3. Hirshfeld surface and fingerprint plot analysis

Hirshfeld surface analysis provides information about the intermolecular interactions of the asymmetric unit with the surrounding molecules in a crystal structure (McKinnon *et al.*, 2007; Spackman & Jayatilaka, 2009). The Hirshfeld surface mapped with d_{norm} and fingerprint plots for each component of the asymmetric unit was generated separately (Figs. 4 and 5) using *CrystalExplorer* (Turner *et al.*, 2017). The strong red region on the Hirshfeld surface indicates the presence N2—H2*b*···O5^{vii}, O8—H8*d*···O1^{v}, O8—H8*c*···O1^{vi}, N1—H1···O7^{iv} and N2—H2*c*···O5^{iii} (the symmetry codes are as in Table 2). Fingerprint plots were generated by combining the

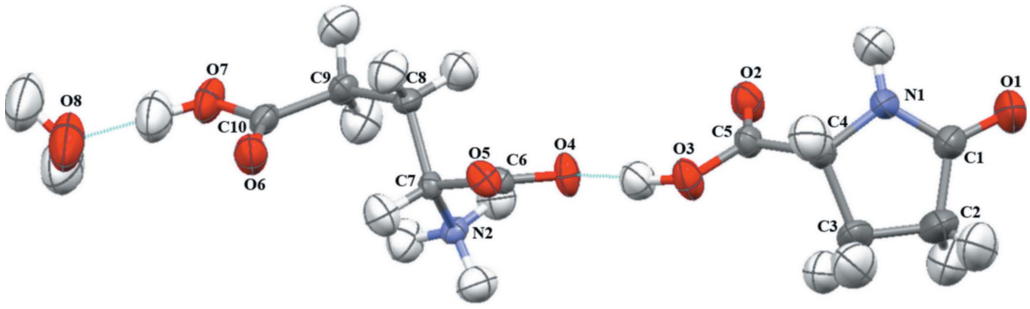

Figure 2
A displacement ellipsoid plot (50% probability level) of the asymmetric unit of (**I**), showing the atom-numbering scheme.

values of the distances of the internal and external atoms (d_i and d_e) in order to analyze the role of intermolecular interactions in the crystal packing based on the Hirshfeld surface. The O···H and H···H intermolecular interactions are the predominant interactions in the case of glutamic acid (66.3 and 28.3%, respectively), pyroglutamic acid (56.2 and 35%) and water (53.1 and 41.8%) (Fig. 5).

3.4. Electrostatic potential

In order to comprehend the participation of noncovalent interactions in the stability of cocrystal (**I**), the electrostatic potential (ESP) has been calculated directly from the electron density (Su & Coppens, 1992). It is the energy required to bring a unit positive charge close to a molecule from infinity, so the ESP calculation contains information about a variety of properties, including energies, as well as properties related to noncovalent interactions (Politzer & Murray, 2002). The three-dimensional electron-density surface coloured according to the electrostatic potential is a convenient way to show the regions of accumulation and depletion of the charge and its gradient. It is helpful in ascertaining the regions of electrophilic and nucleophilic attack. It can also explain the binding affinities in small molecules and in proteins (Kumar *et al.*, 2016; Arputharaj *et al.*, 2012; Yearley *et al.*, 2007; Zhurova *et al.*, 2016; Rajalakshmi *et al.*, 2014; Kalaiarasi *et al.*, 2016).

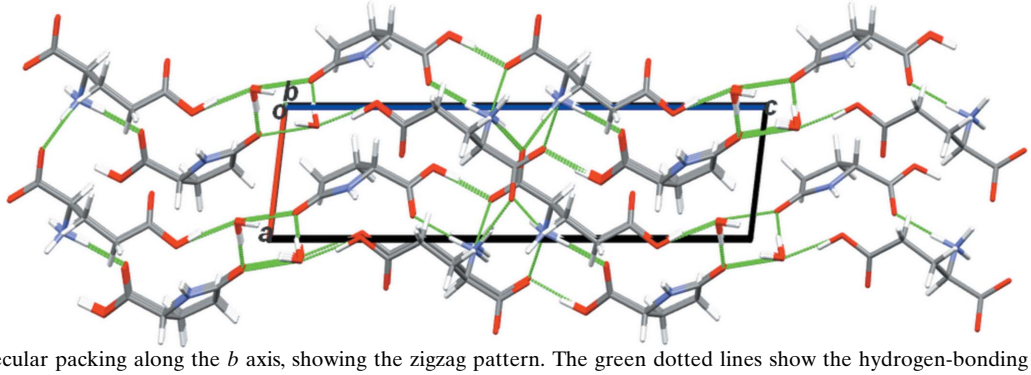

Figure 3
A view of the molecular packing along the *b* axis, showing the zigzag pattern. The green dotted lines show the hydrogen-bonding motif.

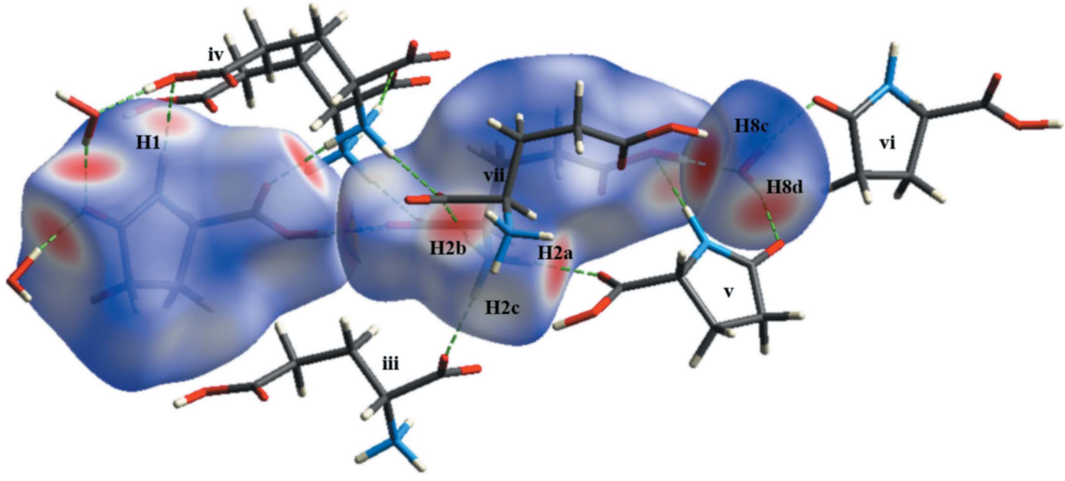

Figure 4
The Hirshfeld surface based on the d_{norm} property of the asymmetric unit around which there is a cluster of interacting molecules. Red and blue colours represent the distances shorter and longer than the sum of the van der Waals radii, and the white colour represents the distances in between. The symmetry codes are the same as in Table 2.

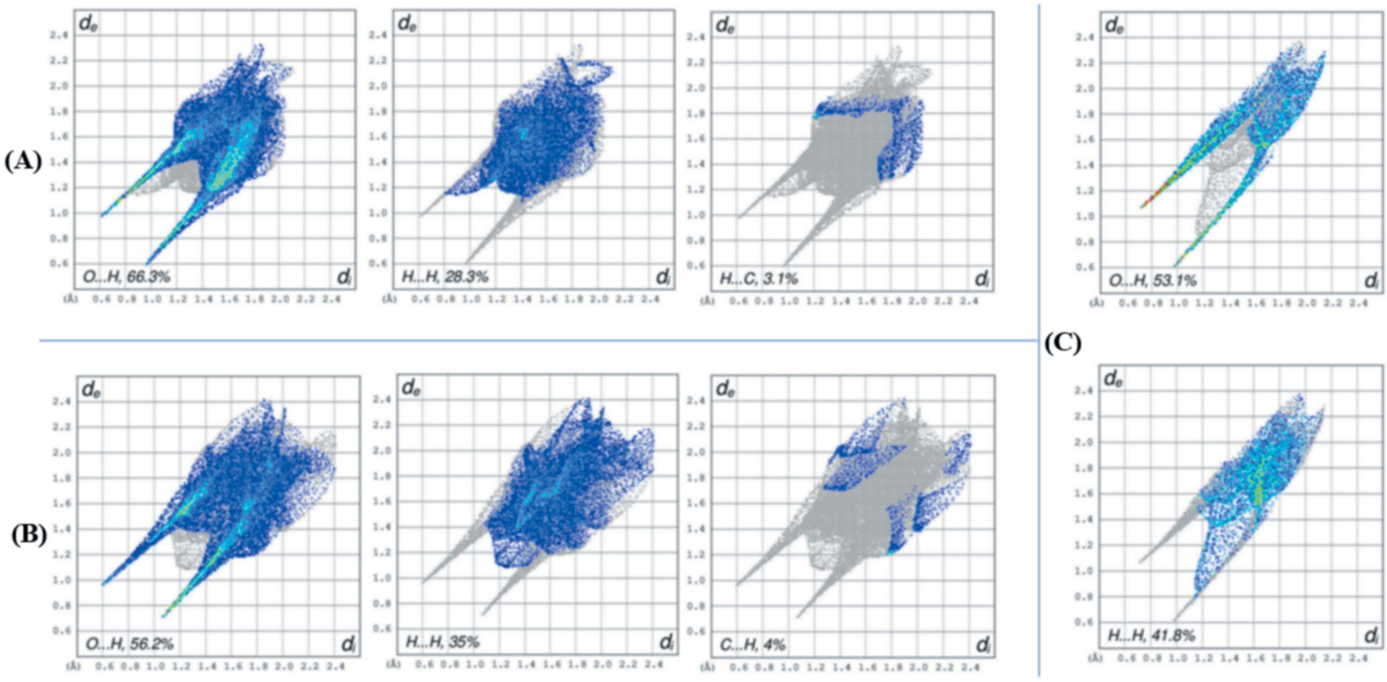

Figure 5
Fingerprint plots presenting the percentage of numerous interactions in glutamic acid (**A**), pyroglutamic acid (**B**) and the water molecule (**C**).

Fig. 6 shows the three-dimensional electron-density surface coloured according to electrostatic potential. There is a qualitative agreement between the transferred and theoretical models. The image shows that the negative charge is spread around the O atoms, while the N atoms are depleted in charge. Carbonyl atom O2 of pyroglutamic acid and O5 of glutamic acid arrange themselves in an opposite *trans* manner. In addition, the charge accumulation on deprotonated atom O4 of glutamic acid attracts the H3 proton from carboxyl atom O3 of pyroglutamic acid, resulting in strong hydrogen-bond formation, which plays a significant role in the stability of these two fragments. On the other hand, water atom O8 acts as an acceptor of a proton from the carboxyl group of glutamic acid and acts as a donor of its H atom with neighbouring components.

3.5. Topology of covalent and intermolecular interactions

The criteria based on simple van der Waals distances is not sufficient to rank the intermolecular interactions. Therefore, in order to make a quantitative analysis and form a hierarchy of intermolecular interactions, a topological analysis was carried out in the realm of AIM theory (Bader, 1990). The critical-point (CP) search of these interactions gave a (3,−1) critical point for the O—H···O, N—H···O and C—H···O hydrogen bonds. Furthermore, the topological analysis of electron density at critical points reveals positive Laplacian values ($\nabla^2\rho_{BCP}$) of electron density for all the above interactions (Gatti, 2005; Gilli *et al.*, 1994; Espinosa & Molins, 2000). According to criteria for hydrogen bonding proposed by Koch & Popelier (1995), the Laplacian of electron density tells us about the nature of the bonds in a molecule. If $\nabla^2\rho_{BCP} > 0$, then the interactions are 'closed shell'; however, if $\nabla^2\rho_{BCP} < 0$, then the interactions are 'open shell'. Table S3 (see supporting information) lists the topological parameters of the covalent bonds and all the values are comparable to those in the literature. Table 3 lists the topological parameters of the intermolecular interactions based on a descending order of electron-density values at the bond critical points. As can be seen, there is a close agreement between the values from the ELMAM2 model and the theoretical model. According to the topological parameters, the classical O—H···O hydrogen bonds are stronger than the N—H···O hydrogen bonds. The strongest interaction is O3—H3···O4 between the glutamic acid and pyroglutamic acid moieties. The hydrogen-bond distance is remarkably short (1.53 Å), with an electron density $\rho_{BCP}(r)$ = 0.480/0.555 e Å^{-3} (ELMAM2/theoretical), which is

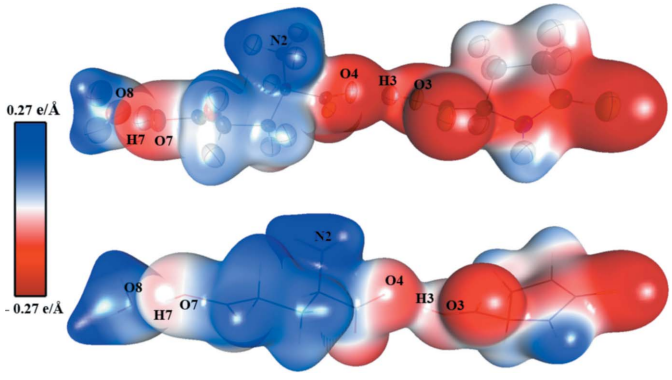

Figure 6
A three-dimensional electron-density surface view of the cocrystal, with the experimental plot (above) and theoretical plot (below) coloured according to electrostatic potential at the 0.05 e Å^{-3} contour level.

Table 3
Topological properties of the (3,−1) CPs in the intermolecular interactions of cocrystal (**I**).

The ELMAM2 values are on the upper line and the theoretical values are on the lower line. The other values shown are: distances (Å), electron density (e Å^{-3}), Laplacian (e Å^{-5}), G_{CP} = bond kinetic-energy density (kJ mol^{-1} Bohr^{-3}) and V_{CP} = bond potential-energy density (kJ mol^{-1} Bohr^{-3}).

No	Bond	d_{12}	d_{1CP}	d_{2BCP}	$\rho_{BCP}(r)$	$\nabla^2\rho_{BCP}(r)$	G_{CP}	V_{CP}
1	O3—H3···O4	1.527	1.059	0.468	0.480	1.533	119.9	−198.1
		1.527	1.041	0.486	0.555	0.51	126.4	−239.0
2	O7—H7···O8	1.569	1.076	0.493	0.435	1.571	106.7	−170.7
		1.566	1.063	0.504	0.485	0.916	110.2	−195.5
3	O8—H8*c*···O1^{vi}	1.787	0.643	1.148	0.287	1.558	67.45	−92.47
		1.789	0.603	1.186	0.266	1.974	70.21	−86.65
4	O8—H8*d*···O1^{v}	1.815	0.662	1.158	0.268	1.551	63.1	−83.97
		1.814	0.620	1.196	0.242	2.16	68.68	−78.52
5	N2—H2*c*···O5^{iii}	1.780	0.624	1.156	0.266	2.042	71.48	−87.33
		1.779	0.631	1.148	0.292	1.444	66.5	−93.67
6	N2—H2*b*···O5^{vii}	1.794	0.633	1.161	0.255	1.956	67.49	−81.71
		1.795	0.640	1.156	0.270	1.804	68.15	−87.15
7	N2—H2*a*···O2^{v}	1.822	0.647	1.176	0.243	1.836	62.97	−75.95
		1.822	0.656	1.167	0.268	1.323	58.84	−81.64
8	N1—H1···O7^{iv}	2.267	0.909	1.363	0.092	0.86	21.49	−19.56
		2.266	0.873	1.394	0.072	1.062	23.16	−17.4
9	C2—H2*e*···O1^{ii}	2.512	1.049	1.465	0.052	0.689	14.76	−10.76
		2.509	1.032	1.480	0.047	0.655	13.84	−9.84
10	C8—H8*a*···O3^{i}	2.556	1.067	1.497	0.048	0.679	14.29	−10.08
		2.555	1.057	1.501	0.045	0.678	14.13	−9.78

Symmetry codes: (i) $-x-1, y-\frac{1}{2}, -z-1$; (ii) $-x-1, y+\frac{1}{2}, -z-2$; (iii) $-x-1, y+\frac{1}{2}, -z-1$; (iv) $-x, y-\frac{1}{2}, -z-1$; (v) $-x, y+\frac{1}{2}, -z-1$; (vi) $x, y, z+1$; (vii) $x+1, y, z$.

significantly elevated. Similarly, the values of the kinetic and potential energy densities are also very high. The next in hierarchy is the O7—H7···O8 interaction between glutamic acid and water molecules, with a hydrogen-bond distance of 1.57 Å and $\rho_{BCP}(r)$ = 0.435/0.485 e Å^{-3}. These two interactions thus have a strong covalent character. In addition, the electrostatic interaction energy calculated using the Buckingham summation method (Buckingham, 1967) *via MoProViewer* (Guillot, 2012) supports the above findings that the electrostatic attraction between pyroglutamic acid and glutamic acid is greater with respect to electrostatic interaction energy (−118.0642 kJ mol^{-1}) compared to that between glutamic acid and water, with a lower electrostatic energy (−91.3719 kJ mol^{-1}). In the intermolecular interactions, the water molecule interacts strongly with two neighbouring pyroglutamic acid molecules *via* O8—H8*d*···O1^{v}, with $\rho_{BCP}(r)$ = 0.268/0.242 e Å^{-3} and $\nabla^2\rho_{BCP}(r)$ = 1.551/2.16 e Å^{-5}, and O8—H8*c*···O1^{vi}, with $\rho_{BCP}(r)$ = 0.287/0.266 e Å^{-3} and $\nabla^2\rho_{BCP}(r)$ = 1.558/1.974 e Å^{-5}, respectively [symmetry codes: (v) $-x, y+\frac{1}{2}, -z-1$; (vi) $x, y, z+1$]. Furthermore, the glutamic acid molecule forms an intermolecular hydrogen bond with two glutamic acid and one pyroglutamic acid molecule through N2—H2*b*···O5^{vii}, N2—H2*c*···O5^{iii}, N2—H2*a*···O2^{v} hydrogen bonds [symmetry codes: (iii) $-x-1, y+\frac{1}{2}, -z-1$; (vii) $x+1, y, z$], with electron-density values $\rho_{BCP}(r)$ = 0.255/0.270, 0.266/0.292 and 0.243/0.268 e Å^{-3}, respectively

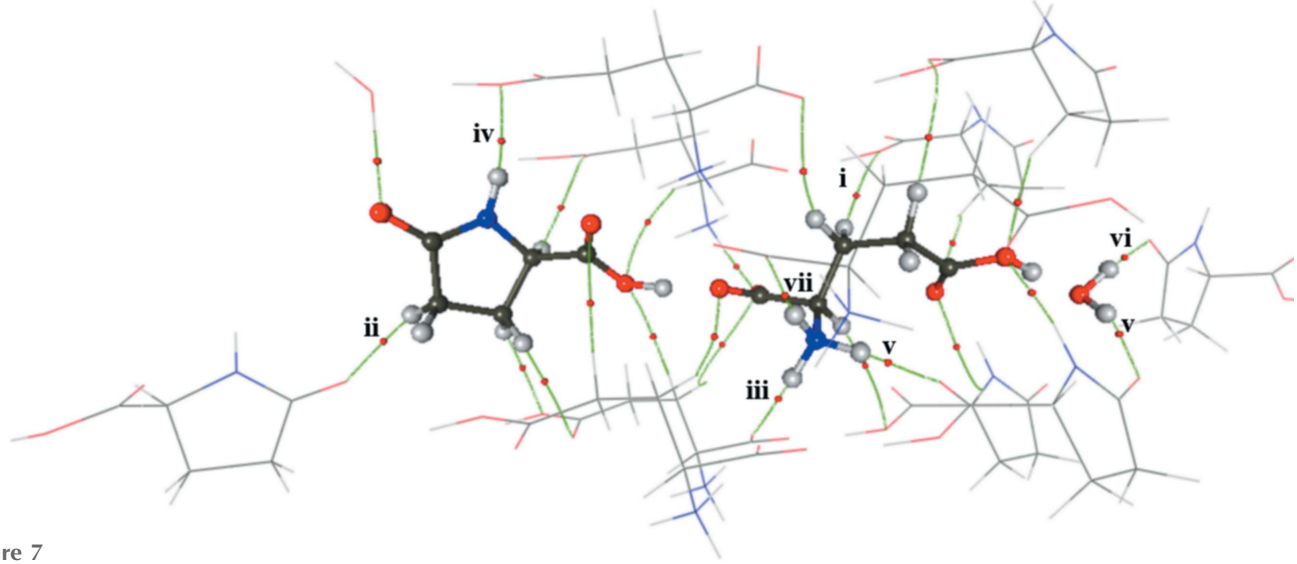

Figure 7
A diagram showing the cluster of cocrystal molecules around reference molecule (**I**), with green lines showing the bond path and red dots showing the critical points. The symmetry codes are the same as in Table 2.

(Table 3). It can be concluded from the topological analysis that the interactions between glutamic acid and pyroglutamic acid are stronger compared to those between glutamic acid and water. It can also be noticed that for the first three interactions in Table 3, the values of the potential energy density are much greater than the values of the kinetic energy density, which indicates that these interactions have a strong covalent character. A cluster of interacting molecules around the parent asymmetric unit, along with bond path (green line) and critical points (red dot), is shown in Fig. 7, while Fig. S3 (see supporting information) shows the Laplacian maps where fine features of the electron-density deformation are clearly visible.

4. Conclusion

We have systematically monitored the transformation of glutamic acid to pyroglutamic acid monohydrate using thermal analysis, hot-stage microscopy and single-crystal X-ray diffraction analysis, which confirms that the process is synchronous, with the melting point occuring around 200 °C. During structural analysis of the solid product obtained after cooling the melt, we came across a cocrystal between the product and the unreacted reactant which provides direct structural evidence of the thermal conversion of glutamic acid to pyroglutamic acid monohydrate. We further carried out a detailed three-dimensional structural analysis of the new cocrystal. The product has strong hydrogen-bonding sites which readily form a cocrystal with unreacted glutamic acid, which exists in the zwitterionic form. The resulting cocrystal is thus very stable. The topological parameters and electrostatic properties calculated using the *transferred model* show a very good agreement with those obtained after multipolar refinement from theoretical structure factors. The topological analysis and the electrostatic interaction energies indicate that the interactions between glutamic acid and pyroglutamic acid are much stronger than those between glutamic acid and water. The study provides three-dimensional structural proof of the thermal conversion of glutamic acid to pyroglutamic acid and highlights the significance of the *transferability principle* for a detailed characterization of the crystal structure.

Acknowledgements

The authors gratefully acknowledge the Higher Education Commission and the Federal Government of Pakistan for funding under the Public Sector Development Programme to establish the Materials Chemistry Laboratory at The Islamia University of Bahawalpur, Pakistan, which made this study possible. The authors thank the referees for their useful remarks.

References

Ahmed, M., Noureen, S., Gros, P. C., Guillot, B. & Jelsch, C. (2011). *Acta Cryst.* C**67**, o329–o333.
Arputharaj, D. S., Hathwar, V. R., Guru Row, T. N. & Kumaradhas, P. (2012). *Cryst. Growth Des.* **12**, 4357–4366.
Bader, R. F. W. (1990). In *Atoms in Molecules: A Quantum Theory*. Oxford: Clarendon Press.
Blöchl, P. E. (1994). *Phys. Rev. B*, **50**, 17953–17979.
Bourhis, L. J., Dolomanov, O. V., Gildea, R. J., Howard, J. A. K. & Puschmann, H. (2015). *Acta Cryst.* A**71**, 59–75.
Brock, C. P., Dunitz, J. D. & Hirshfeld, F. L. (1991). *Acta Cryst.* B**47**, 789–797.
Bruker (2016). *APEX3*, *SAINT* and *SADABS*. Bruker AXS Inc., Madison, Wisconsin, USA.
Buckingham, A. (1967). *Adv. Chem. Phys.* **12**, 107–142.
Ciunik, Z. & Głowiak, T. (1983). *Acta Cryst.* C**39**, 1271–1273.
Coppens, P. (1998). *Acta Cryst.* A**54**, 779–788.
Dittrich, B., Hübschle, C. B., Messerschmidt, M., Kalinowski, R., Girnt, D. & Luger, P. (2005). *Acta Cryst.* A**61**, 314–320.
Dittrich, B., Koritsánszky, T. & Luger, P. (2004). *Angew. Chem. Int. Ed.* **43**, 2718–2721.
Dittrich, B., Munshi, P. & Spackman, M. A. (2007). *Acta Cryst.* B**63**, 505–509.
Dolomanov, O. V., Bourhis, L. J., Gildea, R. J., Howard, J. A. K. & Puschmann, H. (2009). *J. Appl. Cryst.* **42**, 339–341.
Domagała, S., Fournier, B., Liebschner, D., Guillot, B. & Jelsch, C. (2012). *Acta Cryst.* A**68**, 337–351.
Domagała, S. & Jelsch, C. (2008). *J. Appl. Cryst.* **41**, 1140–1149.
Espinosa, E. & Molins, E. (2000). *J. Chem. Phys.* **113**, 5686–5694.
Faroque, M. U., Noureen, S., Mirza, S. H., Tahir, M. N. & Ahmed, M. (2019). *Acta Cryst.* C**75**, 46–53.
Flack, H. D. (1983). *Acta Cryst.* A**39**, 876–881.
Flaig, R., Koritsanszky, T., Dittrich, B., Wagner, A. & Luger, P. (2002). *J. Am. Chem. Soc.* **124**, 3407–3417.
Flaig, R., Koritsánszky, T., Janczak, J., Krane, H. G., Morgenroth, W. & Luger, P. (1999). *Angew. Chem. Int. Ed.* **38**, 1397–1400.
Gatti, C. (2005). *Z. Kristallogr. Cryst. Mater.* **220**, 399–457.
Giannozzi, P., Andreussi, O., Brumme, T., Bunau, O., Buongiorno Nardelli, M., Calandra, M., Car, R., Cavazzoni, C., Ceresoli, D., Cococcioni, M., Colonna, N., Carnimeo, I., Dal Corso, A., de Gironcoli, S., Delugas, P., DiStasio, R. A., Ferretti, A., Floris, A., Fratesi, G., Fugallo, G., Gebauer, R., Gerstmann, U., Giustino, F., Gorni, T., Jia, J., Kawamura, M., Ko, H. Y., Kokalj, A., Küçükbenli, E., Lazzeri, M., Marsili, M., Marzari, N., Mauri, F., Nguyen, N. L., Nguyen, H. V., Otero-de-la-Roza, A., Paulatto, L., Poncé, S., Rocca, D., Sabatini, R., Santra, B., Schlipf, M., Seitsonen, A. P., Smogunov, A., Timrov, I., Thonhauser, T., Umari, P., Vast, N., Wu, X. & Baroni, S. (2017). *J. Phys. Condens. Matter*, **29**, 465901.
Gibson, W. T. & Scott, I. R. (1992). US Patent 515895.
Gilli, P., Bertolasi, V., Ferretti, V. & Gilli, G. (1994). *J. Am. Chem. Soc.* **116**, 909–915.
Grimme, S., Antony, J., Ehrlich, S. & Krieg, H. (2010). *J. Chem. Phys.* **132**, 154104.
Groom, C. R., Bruno, I. J., Lightfoot, M. P. & Ward, S. C. (2016). *Acta Cryst.* B**72**, 171–179.
Guillot, B. (2012). *Acta Cryst.* A**68**, s204.
Haitinger, L. (1882). *Monatsh. Chem.* **3**, 228–229.
Hansen, N. K. & Coppens, P. (1978). *Acta Cryst.* A**34**, 909–921.
He, Y. S., Dufour, J. P. & Meurens, M. (2003). *J. Tea Sci.* **23**, 99–104.
Jelsch, C., Guillot, B., Lagoutte, A. & Lecomte, C. (2005). *J. Appl. Cryst.* **38**, 38–54.
Jelsch, C., Pichon-Pesme, V., Lecomte, C. & Aubry, A. (1998). *Acta Cryst.* D**54**, 1306–1318.
Kalaiarasi, C., Pavan, M. S. & Kumaradhas, P. (2016). *Acta Cryst.* B**72**, 775–786.
Koch, U. & Popelier, P. L. (1995). *J. Phys. Chem.* **99**, 9747–9754.
Krause, L., Herbst-Irmer, R., Sheldrick, G. M. & Stalke, D. (2015). *J. Appl. Cryst.* **48**, 3–10.
Kumar, P. & Maria Dominiak, P. (2016). *Biophys. J.* **110**, 380a.
McKinnon, J. J., Fabbiani, F. P. & Spackman, M. A. (2007). *Cryst. Growth Des.* **7**, 755–769.
Menozzi, A. & Appiani, G. (1892). *Chim. Ital.* **22**, 105–108.
Menozzi, A. & Appiani, G. (1894). *Chim. Ital.* **24**, 370–391.

Mosqueira, F. G., Ramos-Bernal, S. & Negrón-Mendoza, A. (2008). *Biosystems*, **91**, 195–200.
Nagashima, N., Sano, C., Kawakita, T. & Iitaka, Y. (1992*a*). *Anal. Sci.* **8**, 115–117.
Nagashima, N., Sano, C., Kawakita, T. & Iitaka, Y. (1992*b*). *Anal. Sci.* **8**, 119–121.
Neuberger, A. (1936). *Biochem. J.* **30**, 2085–2094.
Nugrahani, I. & Jessica, M. A. (2021). *Molecules*, **26**, 3279.
Perdew, J. P., Burke, K. & Ernzerhof, M. (1996). *Phys. Rev. Lett.* **77**, 3865–3868.
Pichon-Pesme, V., Jelsch, C., Guillot, B. & Lecomte, C. (2004). *Acta Cryst.* A**60**, 204–208.
Pichon-Pesme, V., Lecomte, C. & Lachekar, H. (1995). *J. Phys. Chem.* **99**, 6242–6250.
Politzer, P. & Murray, J. S. (2002). *Theor. Chem. Acc.* **108**, 134–142.
Rajalakshmi, G., Hathwar, V. R. & Kumaradhas, P. (2014). *Acta Cryst.* B**70**, 568–579.
Ruysink, A. F. J. & Vos, A. (1974). *Acta Cryst.* A**30**, 503–506.
Sano, C., Nagashima, N., Kawakita, T. & Iitaka, Y. (1989). *Anal. Sci.* **5**, 121–122.
Shahi, M. N., Iqbal, A., Bibi, R., Khan, M., Ahmed, M. & Noureen, S. (2020). *J. Mol. Struct.* **1206**, 127657.
Sheldrick, G. M. (2008). *Acta Cryst.* A**64**, 112–122.
Sheldrick, G. M. (2015). *Acta Cryst.* C**71**, 3–8.
Shih, F. F. (1985). *J. Chromatogr. A*, **322**, 248–256.
Spackman, M. A. & Jayatilaka, D. (2009). *CrystEngComm*, **11**, 19–32.
Stash, A. I. & Tsirelson, V. G. (2014). *J. Appl. Cryst.* **47**, 2086–2089.
Su, Z. & Coppens, P. (1992). *Acta Cryst.* A**48**, 188–197.
Suzuki, Y., Motoi, H. & Sato, K. (1999). *J. Agric. Food Chem.* **47**, 3248–3251.
Taira, Z. & Watson, W. H. (1977). *Acta Cryst.* B**33**, 3823–3827.
Turner, M. J., McKinnon, J. J., Wolff, S. K., Grimwood, D. J., Spackman, P. R., Jayatilaka, D. & Spackman, M. A. (2017). *CrystalExplorer*. University of Western Australia.
Volkov, A., Li, X., Koritsanszky, T. & Coppens, P. (2004). *J. Phys. Chem. A*, **108**, 4283–4300.
Weiss, I. M., Muth, C., Drumm, R. & Kirchner, H. O. (2018). *BMC Biophys.* **11**, 2. https://doi.org/10.1186/s13628-018-0042-4.
Wilson, H. & Cannan, R. K. (1937). *J. Biol. Chem.* **119**, 309–331.
Yearley, E. J., Zhurova, E. A., Zhurov, V. V. & Pinkerton, A. A. (2007). *J. Am. Chem. Soc.* **129**, 15013–15021.
Zhurova, E. A., Zhurov, V. V., Kumaradhas, P., Cenedese, S. & Pinkerton, A. A. (2016). *J. Phys. Chem. B*, **120**, 8882–8891.

supporting information

Acta Cryst. (2022). C**78**, 72-80 [https://doi.org/10.1107/S2053229621013607]

Thermal-induced transformation of glutamic acid to pyroglutamic acid and self-cocrystallization: a charge–density analysis

Sehrish Akram, Arshad Mehmood, Sajida Noureen and Maqsood Ahmed

Computing details

Cell refinement: *SAINT* (Bruker, 2016) for IAM_SHELX. Data reduction: *SAINT* (Bruker, 2016) for IAM_SHELX. Program(s) used to solve structure: SHELXT2018 (Sheldrick, 2015) for IAM_SHELX. Program(s) used to refine structure: olex2.refine (Bourhis *et al.*, 2015) for IAM_SHELX; MoPro (Jelsch *et al.*, 2005) for ELMAM2_MoPro. Molecular graphics: OLEX2 (Dolomanov *et al.*, 2009) for IAM_SHELX. Software used to prepare material for publication: OLEX2 (Dolomanov *et al.*, 2009) for IAM_SHELX.

2-Aminopentanedioic acid–5-oxopyrrolidine-2-carboxylic acid–water (1/1/1) (IAM_SHELX)

Crystal data

$C_5H_7NO_3 \cdot C_5H_9NO_4 \cdot H_2O$
$M_r = 294.26$
Monoclinic, $P2_1$
$a = 5.1153$ (3) Å
$b = 7.1849$ (4) Å
$c = 18.4639$ (9) Å
$\beta = 96.817$ (2)°
$V = 673.80$ (6) Å^3
$Z = 2$
$F(000) = 312.231$
$D_x = 1.450$ Mg m^{-3}
Mo $K\alpha$ radiation, $\lambda = 0.71073$ Å
Cell parameters from 3695 reflections
$\theta = 3.1$–$25.3°$
$\mu = 0.13$ mm^{-1}
$T = 298$ K
Plate-like, colourless
0.5 × 0.29 × 0.07 mm

Data collection

Bruker D8 Venture diffractometer
φ and ω scans
Absorption correction: multi-scan (SADABS; Bruker, 2016; Krause *et al.*, 2015)
$T_{min} = 0.487$, $T_{max} = 0.745$
7139 measured reflections
2442 independent reflections
1905 reflections with $I \geq 2u(I)$
$R_{int} = 0.055$
$\theta_{max} = 25.3°$, $\theta_{min} = 2.2°$
$h = -6 \rightarrow 6$
$k = -8 \rightarrow 8$
$l = -22 \rightarrow 22$

Refinement

Refinement on F^2
Least-squares matrix: full
$R[F^2 > 2\sigma(F^2)] = 0.051$
$wR(F^2) = 0.116$
$S = 1.12$
2442 reflections
199 parameters
1 restraint
23 constraints
H atoms treated by a mixture of independent and constrained refinement
$w = 1/[\sigma^2(F_o^2) + (0.0331P)^2 + 0.2123P]$ where $P = (F_o^2 + 2F_c^2)/3$
$(\Delta/\sigma)_{max} = 0.0003$
$\Delta\rho_{max} = 0.27$ e Å^{-3}
$\Delta\rho_{min} = -0.27$ e Å^{-3}
Absolute structure: Flack (1983)
Absolute structure parameter: 0.0 (19)

Fractional atomic coordinates and isotropic or equivalent isotropic displacement parameters (Å²)

	x	*y*	*z*	U_{iso}*/U_{eq}
O2	−0.1942 (5)	−0.6634 (4)	−0.70646 (12)	0.0468 (7)
O3	−0.5490 (5)	−0.5139 (4)	−0.67679 (12)	0.0454 (7)
O4	−0.3070 (4)	−0.4779 (4)	−0.54825 (10)	0.0379 (6)
O5	−0.6743 (4)	−0.5020 (3)	−0.49491 (11)	0.0343 (6)
O6	−0.3416 (5)	−0.4878 (4)	−0.25593 (12)	0.0482 (7)
O7	0.0386 (5)	−0.5644 (4)	−0.19112 (12)	0.0506 (8)
O8	−0.1419 (9)	−0.4677 (7)	−0.07159 (18)	0.0867 (12)
N1	−0.4011 (8)	−0.7027 (5)	−0.84719 (15)	0.0520 (10)
N2	−0.0595 (5)	−0.2985 (4)	−0.42950 (13)	0.0265 (6)
H2a	0.018 (3)	−0.264 (2)	−0.38588 (13)	0.0397 (9)*
H2b	0.058 (2)	−0.3540 (9)	−0.4541 (9)	0.0397 (9)*
H2c	−0.1242 (7)	−0.1988 (13)	−0.4541 (10)	0.0397 (9)*
O1	−0.2102 (7)	−0.6781 (4)	−0.95192 (14)	0.0793 (11)
C1	−0.3373 (9)	−0.6116 (6)	−0.9046 (2)	0.0511 (11)
C2	−0.4415 (13)	−0.4213 (7)	−0.9039 (3)	0.0831 (18)
H2d	−0.3007 (13)	−0.3313 (7)	−0.9051 (3)	0.100 (2)*
H2e	−0.5711 (13)	−0.4007 (7)	−0.9459 (3)	0.100 (2)*
C3	−0.5660 (10)	−0.4021 (6)	−0.8346 (2)	0.0565 (12)
H3a	−0.4714 (10)	−0.3116 (6)	−0.8025 (2)	0.0678 (14)*
H3b	−0.7479 (10)	−0.3625 (6)	−0.8450 (2)	0.0678 (14)*
C4	−0.5501 (7)	−0.5953 (5)	−0.79956 (16)	0.0378 (9)
H4	−0.7272 (7)	−0.6477 (5)	−0.80005 (16)	0.0454 (11)*
C5	−0.4099 (7)	−0.5955 (5)	−0.72237 (17)	0.0337 (8)
C6	−0.4334 (6)	−0.4712 (5)	−0.49441 (16)	0.0275 (7)
C7	−0.2773 (6)	−0.4305 (4)	−0.42022 (15)	0.0244 (7)
H7a	−0.3944 (6)	−0.3754 (4)	−0.38777 (15)	0.0293 (9)*
C8	−0.1729 (7)	−0.6164 (5)	−0.38876 (16)	0.0319 (8)
H8a	−0.3230 (7)	−0.6946 (5)	−0.38229 (16)	0.0383 (9)*
H8b	−0.0782 (7)	−0.6763 (5)	−0.42487 (16)	0.0383 (9)*
C9	0.0067 (7)	−0.6130 (5)	−0.31693 (15)	0.0353 (8)
H9a	0.0735 (7)	−0.7378 (5)	−0.30658 (15)	0.0423 (10)*
H9b	0.1562 (7)	−0.5335 (5)	−0.32252 (15)	0.0423 (10)*
C10	−0.1211 (8)	−0.5462 (5)	−0.25318 (17)	0.0363 (9)
H7	−0.042 (7)	−0.536 (6)	−0.152 (2)	0.0544 (13)*
H1	−0.339 (7)	−0.827 (6)	−0.832 (2)	0.0544 (13)*
H3	−0.467 (7)	−0.497 (7)	−0.628 (2)	0.0544 (13)*
H8c	−0.126 (12)	−0.552 (11)	−0.031 (4)	0.15 (3)*
H8d	0.010 (12)	−0.395 (8)	−0.058 (3)	0.10 (2)*

Atomic displacement parameters (Å²)

	U^{11}	U^{22}	U^{33}	U^{12}	U^{13}	U^{23}
O2	0.0454 (16)	0.0587 (18)	0.0343 (13)	0.0148 (14)	−0.0034 (12)	−0.0035 (13)
O3	0.0459 (14)	0.0590 (18)	0.0302 (12)	0.0106 (15)	0.0004 (11)	−0.0112 (13)
O4	0.0310 (12)	0.0594 (17)	0.0228 (10)	−0.0007 (13)	0.0010 (9)	−0.0082 (12)

O5	0.0235 (12)	0.0396 (15)	0.0386 (12)	−0.0029 (12)	−0.0012 (9)	−0.0086 (12)
O6	0.0520 (16)	0.0563 (18)	0.0369 (13)	0.0077 (16)	0.0073 (11)	−0.0001 (14)
O7	0.0560 (17)	0.065 (2)	0.0288 (12)	−0.0069 (15)	−0.0021 (12)	0.0038 (14)
O8	0.117 (3)	0.102 (3)	0.0429 (18)	−0.029 (3)	0.0159 (18)	−0.001 (2)
N1	0.099 (3)	0.0292 (19)	0.0283 (16)	0.0117 (19)	0.0090 (17)	−0.0004 (15)
N2	0.0283 (14)	0.0246 (14)	0.0257 (13)	−0.0054 (12)	−0.0003 (11)	0.0011 (12)
O1	0.133 (3)	0.067 (2)	0.0440 (16)	0.024 (2)	0.0347 (18)	0.0022 (17)
C1	0.077 (3)	0.041 (2)	0.0340 (19)	0.004 (2)	0.002 (2)	0.003 (2)
C2	0.147 (5)	0.049 (3)	0.058 (3)	0.029 (3)	0.031 (3)	0.015 (2)
C3	0.079 (3)	0.046 (3)	0.042 (2)	0.021 (2)	−0.005 (2)	0.004 (2)
C4	0.049 (2)	0.034 (2)	0.0290 (16)	0.0029 (18)	−0.0023 (16)	−0.0014 (17)
C5	0.040 (2)	0.0312 (19)	0.0291 (16)	−0.0007 (17)	0.0005 (15)	−0.0001 (16)
C6	0.0288 (17)	0.0223 (17)	0.0310 (16)	0.0018 (14)	0.0018 (13)	−0.0009 (15)
C7	0.0250 (17)	0.0257 (18)	0.0229 (15)	−0.0044 (13)	0.0043 (13)	−0.0027 (14)
C8	0.040 (2)	0.0250 (18)	0.0308 (17)	−0.0018 (16)	0.0050 (14)	0.0009 (16)
C9	0.040 (2)	0.034 (2)	0.0302 (16)	0.0059 (17)	−0.0030 (15)	0.0044 (16)
C10	0.047 (2)	0.029 (2)	0.0324 (18)	−0.0048 (17)	0.0032 (16)	0.0067 (16)

Geometric parameters (Å, º)

O2—C5	1.210 (4)	O1—C1	1.244 (5)
O3—C5	1.304 (4)	C1—C2	1.468 (6)
O4—C6	1.249 (3)	C2—C3	1.502 (6)
O5—C6	1.251 (3)	C3—C4	1.530 (5)
O6—C10	1.198 (4)	C4—C5	1.518 (5)
O7—C10	1.333 (4)	C6—C7	1.530 (4)
N1—C1	1.320 (5)	C7—C8	1.527 (4)
N1—C4	1.452 (5)	C8—C9	1.521 (4)
N2—C7	1.488 (4)	C9—C10	1.492 (4)
C4—N1—C1	114.9 (3)	O5—C6—O4	126.1 (3)
O1—C1—N1	125.0 (4)	C7—C6—O4	117.1 (3)
C2—C1—N1	109.3 (4)	C7—C6—O5	116.7 (3)
C2—C1—O1	125.8 (4)	C6—C7—N2	109.7 (2)
C3—C2—C1	106.5 (4)	C8—C7—N2	111.6 (2)
C4—C3—C2	105.7 (3)	C8—C7—C6	107.2 (2)
C3—C4—N1	103.4 (3)	C9—C8—C7	117.7 (3)
C5—C4—N1	110.2 (3)	C10—C9—C8	114.6 (3)
C5—C4—C3	113.2 (3)	O7—C10—O6	123.3 (3)
O3—C5—O2	125.2 (3)	C9—C10—O6	125.3 (3)
C4—C5—O2	122.9 (3)	C9—C10—O7	111.4 (3)
C4—C5—O3	111.9 (3)		
O2—C5—C4—N1	5.8 (4)	O7—C10—C9—C8	173.7 (3)
O2—C5—C4—C3	−109.3 (4)	N1—C1—C2—C3	3.6 (4)
O3—C5—C4—N1	−174.5 (3)	N1—C4—C3—C2	4.7 (4)
O3—C5—C4—C3	70.3 (3)	N2—C7—C8—C9	55.7 (3)
O4—C6—C7—N2	35.1 (3)	O1—C1—C2—C3	−176.8 (6)

O4—C6—C7—C8	−86.2 (3)	C1—C2—C3—C4	−5.1 (5)
O5—C6—C7—N2	−147.6 (3)	C2—C3—C4—C5	123.8 (4)
O5—C6—C7—C8	91.0 (3)	C6—C7—C8—C9	175.8 (2)
O6—C10—C9—C8	−4.3 (4)	C7—C8—C9—C10	64.9 (3)

2-Aminopentanedioic acid–5-oxopyrrolidine-2-carboxylic acid–water (1/1/1) (ELMAM2_MoPro)

Crystal data

$C_5H_7NO_3·C_5H_9NO_4·H_2O$
M_r = 294.25
Monoclinic, $P2_1$
a = 5.1153 (3) Å
b = 7.1849 (4) Å
c = 18.4639 (9) Å
β = 96.817 (2)°
V = 673.80 (6) Å^3
Z = 2
$F(000)$ = 312
D_x = 1.451 Mg m^{-3}
Mo $K\alpha$ radiation, λ = 0.71073 Å
Cell parameters from 3695 reflections
θ = 2.2–26.4°
μ = 0.13 mm^{-1}
T = 298 K
Plate-like, colourless
0.5 × 0.29 × 0.07 mm

Data collection

Bruker D8 Venture diffractometer
Radiation source: fine-focus sealed tube
Helios Mirror Optics monochromator
ω and phi scan
Absorption correction: multi-scan (SADABS; Bruker, 2016)
T_{min} = 0.487, T_{max} = 0.745
7139 measured reflections
2373 independent reflections
1855 reflections with $I > 2\ \sigma(I)$
R_{int} = 0.055
θ_{max} = 25.3°, θ_{min} = 2.2°
h = −6→6
k = −8→8
l = 0→22

Refinement

Refinement on F^2
Least-squares matrix: full
$R[F^2 > 2\sigma(F^2)]$ = 0.046
$wR(F^2)$ = 0.096
S = 0.85
2373 reflections
120 parameters
0 restraints
Primary atom site location: structure-invariant direct methods
Secondary atom site location: difference Fourier map
Hydrogen site location: difference Fourier map
H-atom parameters constrained
$w = 1/[\sigma^2(F_o^2) + (0.03314P)^2 + 0.21229P]$ where $P = (F_o^2 + 2F_c^2$
$(\Delta/\sigma)_{max}$ < 0.001
$\Delta\rho_{max}$ = 0.24 e Å−3
$\Delta\rho_{min}$ = −0.25 e Å−3
Absolute structure: Flack (1983)
Absolute structure parameter: 0.0 (19)

Special details

Refinement. Refinement of F^2 against reflections. The threshold expression of $F^2 > 2$sigma(F^2) is used for calculating R-factors(gt) and is not relevant to the choice of reflections for refinement. R-factors based on F^2 are statistically about twice as large as those based on F, and R-factors based on ALL data will be even larger.
The diffraction data was collected on a Bruker D8 Venture with PHOTON II Detector single crystal X-rays diffractometer at room temperature (298K) using source of Mo K radiations (λ = 0.71073 Å). The data was processed using the SAINT (Bruker, 2016) program and absorption correction was done with SADABS program (Krause *et al.*, 2015).

Fractional atomic coordinates and isotropic or equivalent isotropic displacement parameters (Å²)

	x	*y*	*z*	U_{iso}*/U_{eq}
O2	−0.1949 (5)	−0.66352 (4)	−0.70660 (12)	0.0449 (8)
O3	−0.5487 (4)	−0.5144 (5)	−0.67669 (11)	0.0427 (7)
O4	−0.3069 (4)	−0.4786 (6)	−0.54831 (10)	0.0364 (6)
O5	−0.6742 (4)	−0.5025 (5)	−0.49480 (11)	0.0326 (6)
O6	−0.3418 (5)	−0.4881 (5)	−0.25599 (11)	0.0460 (8)
O7	0.0377 (5)	−0.5645 (5)	−0.19089 (10)	0.0477 (8)
O8	−0.1412 (7)	−0.4681 (7)	−0.07136 (14)	0.0839 (13)
N1	−0.4016 (7)	−0.7037 (6)	−0.84719 (14)	0.0494 (13)
N2	−0.0593 (5)	−0.2985 (5)	−0.42953 (13)	0.0233 (7)
H2a	0.02779	−0.25631	−0.37858	0.04989
H2b	0.08057	−0.36351	−0.45860	0.04642
H2c	−0.13633	−0.18110	−0.45736	0.04816
O1	−0.2104 (7)	−0.6786 (6)	−0.95178 (13)	0.0762 (14)
C1	−0.3381 (9)	−0.6124 (7)	−0.90487 (19)	0.0475 (14)
C2	−0.4439 (12)	−0.4228 (8)	−0.9039 (3)	0.080 (2)
H2d	−0.28769	−0.31874	−0.90416	0.08108
H2e	−0.59363	−0.39729	−0.95040	0.08615
C3	−0.5665 (9)	−0.4022 (7)	−0.8348 (2)	0.0525 (15)
H3a	−0.46015	−0.29823	−0.79972	0.06485
H3b	−0.77012	−0.35761	−0.84797	0.07379
C4	−0.5502 (7)	−0.5963 (6)	−0.79962 (15)	0.0354 (11)
H4	−0.74871	−0.65370	−0.80134	0.06309
C5	−0.4105 (7)	−0.5959 (6)	−0.72228 (16)	0.0303 (10)
C6	−0.4335 (6)	−0.4713 (6)	−0.49452 (15)	0.0234 (8)
C7	−0.2771 (6)	−0.4300 (6)	−0.42021 (15)	0.0214 (8)
H7a	−0.40471	−0.36785	−0.38373	0.04695
C8	−0.1734 (7)	−0.6172 (6)	−0.38898 (15)	0.0285 (10)
H8a	−0.34072	−0.70475	−0.38055	0.05197
H8b	−0.06218	−0.68294	−0.42869	0.04922
C9	0.0074 (6)	−0.6141 (6)	−0.31685 (16)	0.0328 (10)
H9a	0.08318	−0.75514	−0.30609	0.06088
H9b	0.17297	−0.52254	−0.32425	0.05664
C10	−0.1217 (7)	−0.5464 (6)	−0.25300 (16)	0.0330 (11)
H7	−0.05506	−0.53002	−0.14644	0.06872
H1	−0.33635	−0.83244	−0.83096	0.07025
H3	−0.46134	−0.49295	−0.62412	0.04348
H8c	−0.12148	−0.55508	−0.02919	0.09454
H8d	0.01745	−0.39122	−0.05805	0.08796

Atomic displacement parameters (Å²)

	U^{11}	U^{22}	U^{33}	U^{12}	U^{13}	U^{23}
O2	0.0455 (16)	0.0563 (18)	0.0309 (13)	0.0140 (14)	−0.0042 (11)	−0.0056 (13)
O3	0.0422 (14)	0.0569 (18)	0.0278 (11)	0.0102 (14)	−0.0008 (10)	−0.0109 (13)
O4	0.0285 (12)	0.0594 (17)	0.0206 (10)	−0.0011 (13)	0.0010 (9)	−0.0084 (12)

O5	0.0214 (12)	0.0394 (14)	0.0358 (11)	−0.0032 (12)	−0.0008 (9)	−0.0096 (12)
O6	0.0495 (15)	0.0554 (18)	0.0334 (12)	0.0109 (15)	0.0066 (11)	−0.0002 (14)
O7	0.0542 (16)	0.062 (2)	0.0248 (11)	−0.0085 (14)	−0.0041 (11)	0.0060 (13)
O8	0.115 (3)	0.099 (3)	0.0394 (14)	−0.029 (2)	0.0157 (14)	−0.0012 (18)
N1	0.095 (3)	0.0280 (18)	0.0262 (14)	0.0110 (18)	0.0092 (16)	−0.0009 (14)
N2	0.0244 (14)	0.0219 (14)	0.0231 (12)	−0.0059 (11)	0.0006 (11)	0.0018 (12)
H2a	0.05087	0.05550	0.04111	−0.01113	−0.00365	−0.00304
H2b	0.03792	0.05235	0.04969	−0.00147	0.00812	−0.00037
H2c	0.05304	0.04055	0.04939	−0.00055	−0.00012	0.00437
O1	0.131 (3)	0.063 (2)	0.0399 (14)	0.026 (2)	0.0335 (17)	0.0030 (16)
C1	0.074 (3)	0.036 (2)	0.0323 (18)	0.007 (2)	0.0065 (19)	0.0039 (19)
C2	0.146 (5)	0.043 (3)	0.056 (3)	0.028 (3)	0.033 (3)	0.017 (2)
H2d	0.12095	0.06835	0.05501	0.00304	0.01489	0.00477
H2e	0.13176	0.07920	0.04270	0.02152	−0.00958	0.00158
C3	0.079 (3)	0.040 (2)	0.036 (2)	0.022 (2)	−0.003 (2)	0.0054 (19)
H3a	0.09291	0.05398	0.04521	0.00519	−0.00192	−0.00064
H3b	0.08819	0.07377	0.05443	0.02321	−0.01218	0.00286
C4	0.050 (2)	0.030 (2)	0.0232 (15)	0.0033 (18)	−0.0058 (16)	−0.0006 (16)
H4	0.07224	0.06272	0.05093	0.00216	−0.00676	−0.00713
C5	0.033 (2)	0.0333 (19)	0.0233 (15)	0.0042 (16)	−0.0015 (15)	−0.0023 (16)
C6	0.0216 (16)	0.0231 (17)	0.0251 (15)	0.0000 (14)	0.0014 (13)	−0.0046 (14)
C7	0.0225 (16)	0.0237 (18)	0.0178 (14)	−0.0032 (13)	0.0010 (12)	−0.0022 (13)
H7a	0.04382	0.05340	0.04476	0.00260	0.01002	−0.00766
C8	0.039 (2)	0.0205 (18)	0.0258 (15)	−0.0007 (15)	0.0020 (14)	0.0028 (15)
H8a	0.05005	0.05407	0.05201	−0.01213	0.00700	0.00516
H8b	0.05035	0.05360	0.04430	0.00986	0.00809	0.00146
C9	0.037 (2)	0.033 (2)	0.0265 (15)	0.0068 (17)	−0.0009 (14)	0.0034 (16)
H9a	0.07445	0.05545	0.05063	0.00968	−0.00136	0.00914
H9b	0.04913	0.06761	0.05163	−0.00999	−0.00042	0.00391
C10	0.041 (2)	0.032 (2)	0.0256 (17)	−0.0015 (17)	0.0002 (16)	0.0059 (15)
H7	0.08678	0.07925	0.03919	−0.00823	0.00352	−0.00048
H1	0.10913	0.05286	0.04978	0.02096	0.01363	−0.00102
H3	0.04304	0.04725	0.03882	0.00719	−0.00062	−0.00379
H8c	0.13941	0.10077	0.04272	−0.01619	0.00776	0.00748
H8d	0.11437	0.09487	0.05149	−0.02124	−0.00321	−0.00610

Geometric parameters (Å, º)

O2—C5	1.208 (4)	C1—C2	1.466 (6)
O3—C5	1.301 (4)	C2—C3	1.493 (6)
O3—H3	1.0310	C2—H2d	1.0948
O4—C6	1.249 (3)	C2—H2e	1.0962
O5—C6	1.251 (3)	C3—C4	1.536 (5)
O6—C10	1.196 (4)	C3—H3b	1.0894
O7—C10	1.332 (4)	C3—H3a	1.0913
O7—H7	1.0260	C4—C5	1.519 (4)
O8—H8d	0.9880	C4—H4	1.0931
O8—H8c	0.9943	C6—C7	1.533 (4)

N1—C1	1.324 (5)	C7—C8	1.533 (4)
N1—C4	1.451 (4)	C7—H7a	1.0879
N1—H1	1.0161	C8—C9	1.529 (4)
N2—C7	1.486 (4)	C8—H8b	1.0880
N2—H2a	1.0373	C8—H8a	1.0881
N2—H2c	1.0409	C9—C10	1.499 (4)
N2—H2b	1.0529	C9—H9b	1.0940
O1—C1	1.240 (5)	C9—H9a	1.0944

C5—O3—H3	117.9	C5—C4—C3	113.1 (3)
C10—O7—H7	111.8	C5—C4—H4	111.1
H8d—O8—H8c	98.8	C3—C4—H4	109.1
C1—N1—C4	114.8 (3)	O3—C5—O2	125.2 (3)
C1—N1—H1	125.8	O3—C5—C4	112.2 (2)
C4—N1—H1	118.9	O2—C5—C4	122.6 (3)
C7—N2—H2a	109.1	O4—C6—O5	126.3 (2)
C7—N2—H2c	109.1	O4—C6—C7	117.1 (2)
C7—N2—H2b	110.0	O5—C6—C7	116.6 (2)
H2a—N2—H2c	107.9	N2—C7—C6	109.8 (2)
H2a—N2—H2b	110.3	N2—C7—C8	111.7 (2)
H2c—N2—H2b	110.4	N2—C7—H7a	108.9
O1—C1—N1	124.8 (3)	C6—C7—C8	106.7 (2)
O1—C1—C2	126.2 (3)	C6—C7—H7a	110.2
N1—C1—C2	108.9 (3)	C8—C7—H7a	109.5
C1—C2—C3	107.2 (3)	C7—C8—C9	117.5 (2)
C1—C2—H2d	111.3	C7—C8—H8b	108.2
C1—C2—H2e	111.7	C7—C8—H8a	108.6
C3—C2—H2d	108.5	C9—C8—H8b	106.4
C3—C2—H2e	109.1	C9—C8—H8a	106.8
H2d—C2—H2e	108.9	H8b—C8—H8a	109.2
C4—C3—C2	105.3 (3)	C10—C9—C8	114.3 (2)
C4—C3—H3b	111.3	C10—C9—H9b	108.8
C4—C3—H3a	111.8	C10—C9—H9a	109.7
C2—C3—H3b	109.1	C8—C9—H9b	107.3
C2—C3—H3a	110.2	C8—C9—H9a	108.0
H3b—C3—H3a	109.1	H9b—C9—H9a	108.5
N1—C4—C5	110.4 (2)	O7—C10—O6	123.4 (3)
N1—C4—C3	103.5 (3)	O7—C10—C9	111.3 (2)
N1—C4—H4	109.5	O6—C10—C9	125.3 (3)

O2—C5—O3—H3	6.84	O1—C1—C2—H2e	64.34
O2—C5—C4—N1	6.0 (6)	C1—N1—C4—C5	−124.1 (6)
O2—C5—C4—C3	−109.4 (6)	C1—N1—C4—C3	−2.8 (5)
O2—C5—C4—H4	127.60	C1—N1—C4—H4	113.39
O3—C5—C4—N1	−174.5 (7)	C1—C2—C3—C4	−5.5 (7)
O3—C5—C4—C3	70.2 (7)	C1—C2—C3—H3b	−125.05
O3—C5—C4—H4	−52.86	C1—C2—C3—H3a	115.27
O4—C6—C7—N2	35.1 (7)	C2—C1—N1—C4	−0.7 (7)

O4—C6—C7—C8	−86.1 (7)	C2—C1—N1—H1	−172.48
O4—C6—C7—H7a	155.06	C2—C3—C4—C5	124.4 (8)
O5—C6—C7—N2	−148.0 (7)	C2—C3—C4—H4	−111.51
O5—C6—C7—C8	90.8 (7)	H2d—C2—C3—C4	−125.80
O5—C6—C7—H7a	−28.01	H2d—C2—C3—H3b	114.63
O6—C10—O7—H7	3.40	H2d—C2—C3—H3a	−5.05
O6—C10—C9—C8	−4.2 (7)	H2e—C2—C3—C4	115.66
O6—C10—C9—H9b	115.73	H2e—C2—C3—H3b	−3.91
O6—C10—C9—H9a	−125.74	H2e—C2—C3—H3a	−123.59
O7—C10—C9—C8	173.8 (7)	C3—C4—N1—H1	169.63
O7—C10—C9—H9b	−66.28	H3a—C3—C4—C5	4.69
O7—C10—C9—H9a	52.25	H3a—C3—C4—H4	128.83
N1—C1—C2—C3	4.0 (6)	H3b—C3—C4—C5	−117.58
N1—C1—C2—H2d	122.48	H3b—C3—C4—H4	6.55
N1—C1—C2—H2e	−115.47	C4—C5—O3—H3	−172.69
N1—C4—C3—C2	4.9 (6)	H4—C4—N1—H1	−74.20
N1—C4—C3—H3b	123.00	C5—C4—N1—H1	48.37
N1—C4—C3—H3a	−114.73	C6—C7—C8—C9	175.7 (5)
N2—C7—C8—C9	55.8 (5)	C6—C7—C8—H8b	55.30
N2—C7—C8—H8b	−64.68	C6—C7—C8—H8a	−63.09
N2—C7—C8—H8a	176.93	C7—C8—C9—C10	64.8 (5)
H2a—N2—C7—C6	171.68	C7—C8—C9—H9b	−56.00
H2a—N2—C7—C8	−70.14	C7—C8—C9—H9a	−172.76
H2a—N2—C7—H7a	50.93	H7a—C7—C8—C9	−64.98
H2b—N2—C7—C6	−67.16	H7a—C7—C8—H8b	174.58
H2b—N2—C7—C8	51.02	H7a—C7—C8—H8a	56.20
H2b—N2—C7—H7a	172.09	H8a—C8—C9—C10	−57.33
H2c—N2—C7—C6	54.02	H8a—C8—C9—H9b	−178.11
H2c—N2—C7—C8	172.19	H8a—C8—C9—H9a	65.13
H2c—N2—C7—H7a	−66.74	H8b—C8—C9—C10	−173.83
O1—C1—N1—C4	179.5 (6)	H8b—C8—C9—H9b	65.39
O1—C1—N1—H1	7.71	H8b—C8—C9—H9a	−51.37
O1—C1—C2—C3	−176.2 (7)	C9—C10—O7—H7	−174.64
O1—C1—C2—H2d	−57.72		

Hydrogen-bond geometry (Å, º)

D—H···*A*	*D*—H	H···*A*	*D*···*A*	*D*—H···*A*
C8—H8*a*···O3^{i}	1.09	2.56	3.471 (4)	141
C2—H2*e*···O1^{ii}	1.10	2.51	3.491 (6)	148
N2—H2*c*···O5^{iii}	1.04	1.78	2.808 (3)	169
N1—H1···O7^{iv}	1.02	2.27	3.220 (4)	156
N2—H2*a*···O2^{v}	1.04	1.83	2.859 (3)	175
O8—H8*d*···O1^{v}	0.99	1.82	2.749 (5)	156
C7—H7*a*···O6	1.09	2.50	3.117 (3)	115
O7—H7···O8	1.03	1.57	2.582 (4)	169
O3—H3···O4	1.03	1.53	2.553 (3)	173
O3—H3···C6	1.03	2.38	3.360 (3)	157

O8—H8*c*···O1^{vi}	0.99	1.79	2.734 (4)	158
O8—H8*c*···C1^{vi}	0.99	2.70	3.504 (4)	139
N2—H2*b*···O5^{vii}	1.05	1.79	2.836 (3)	170

Symmetry codes: (i) −*x*−1, *y*−1/2, −*z*−1; (ii) −*x*−1, *y*+1/2, −*z*−2; (iii) −*x*−1, *y*+1/2, −*z*−1; (iv) −*x*, *y*−1/2, −*z*−1; (v) −*x*, *y*+1/2, −*z*−1; (vi) *x*, *y*, *z*+1; (vii) *x*+1, *y*, *z*.